A three-dimensional self-consistent computer simulation of a geomagnetic field reversal

Gary A. Glatzmaier* **& Paul H. Roberts†**

* Institute of Geophysics and Planetary Physics, Los Alamos National Laboratory, Los Alamos, New Mexico 87454, USA
† Institute of Geophysics and Planetary Physics, University of California, Los Angeles, California 90024, USA

A three-dimensional, self-consistent numerical model of the geodynamo is described, that maintains a magnetic field for over 40,000 years. The model, which incorporates a finitely conducting inner core, undergoes several polarity excursions and then, near the end of the simulation, a successful reversal of the dipole moment. This simulated magnetic field reversal shares some features with real reversals of the geomagnetic field, and may provide insight into the geomagnetic reversal mechanism.

A FUNDAMENTAL goal of geophysics is a coherent understanding of the structure and dynamics of the Earth's interior. An integral part of this understanding must be a model of the Earth's magnetic field that reproduces its salient features: a field that is maintained for many magnetic diffusion times, is dominantly dipolar at the surface with a dipole axis that on the average lies close to the geographic axis of rotation, and exhibits secular variation with occasional excursions and reversals. The only plausible candidate for such a model is the dynamo model, in which new magnetic field is continually being generated by the shearing and twisting fluid motions within the Earth's liquid, electrically conducting, outer core[1,2]. According to ref. 3, Albert Einstein considered understanding the origin of the Earth's magnetic field as being one of the five most important unsolved problems in physics. Today we know that a nonlinear three-dimensional model of the magnetohydrodynamics (MHD) of the Earth's core is needed to explain the structure and the long-term evolution of the geomagnetic field.

There are two principal reasons for this. First, it is widely perceived that linear mathematical analysis, which has provided great insights into basic dynamo processes, is unlikely to contribute as fundamentally to the understanding of the geodynamo because the Earth operates in the so-called 'strong-field' regime. Analytical methods are successful in studying 'weak-field' regimes, in which the magnetic forces can be treated as a perturbation in the dynamics. However, in the strong-field regime the nonlinear magnetic Lorentz force is as large as the Coriolis force and therefore cannot be treated as a perturbation. A nonlinear numerical computation is therefore required to simulate the MHD.

The second reason arises from Cowling's theorem[4], which shows that a self-sustained magnetic field produced by a dynamo cannot be axisymmetric. But most numerical models of dynamos have been 'mean-field' kinematic models, which require a prescription of the axisymmetric effects of some hypothetical three-dimensional convection and solve for the evolution of only the two-dimensional axisymmetric parts of the magnetic fields[5]. Intermediate mean-field models[6 11] go somewhat further by also solving for the axisymmetric zonal flow and meridional circulation, but still require a prescribed two-dimensional structure of some hypothetical averaged helical flow (the alpha effect[2]) and usually a prescribed structure for the buoyancy force or for the zonal thermal wind shear it produces (the omega effect[1]). They are therefore not self-consistent because the solutions strongly depend on how one chooses to prescribe the alpha and omega structures. The simplest way to generate a three-dimensional magnetic field is to drive it with a prescribed three-dimensional velocity profile[12 14]; but in this approach the (kinematic) velocity is not a self-consistent convective solution with nonlinear feedback from the Lorentz force. Travelling-wave solutions can also be generated[15] but lack mode-dependent temporal behaviour. Magneto-convection simulations in three dimensions are closer to self-consistency because the time-dependent thermodynamic, velocity, and magnetic fields are all solved in three dimensions with nonlinear feedback[16 19]; but the main part of the magnetic field is maintained via boundary conditions. These approaches have been used because of their simplicity and relatively small computing resource requirements; but they are limited because either they do not produce self-consistent solutions of the full three-dimensional MHD equations or, in magneto-convection, they do not produce self-sustaining magnetic fields and are therefore not suitable for studying field reversals. They have been and continue to be extremely useful for providing a relatively cheap way of testing the influence of new physics[9] or studying secular variation of the field on short timescales[19].

Self-consistent numerical simulations of three-dimensional convective dynamos have been computed in planar (cartesian) geometry to study local dynamo action[20 23] and in global (spherical) geometry[24 29] to study the solar dynamo. Of these, however, the only models that generate magnetic energy an order of magnitude greater than kinetic energy and therefore begin to approach the strong-field regime appropriate for studying the geodynamo are the recent models by St Pierre[23] and Kageyama *et al.*[29]. In the other models, the generated magnetic energy is several orders of magnitude less than the kinetic energy.

Here we present a fully self-consistent three-dimensional numerical simulation of a convective strong-field dynamo in a spherical shell with a finitely conducting inner core[30]. A magnetic field is maintained for more than three magnetic diffusion times and has energy at least three orders of magnitude greater than the kinetic energy of the convection that maintains it. The exciting feature that we focus on in this paper is a reversal of the dipole polarity that occurs near the end of our simulation. The simulation required over 2,000,000 computational time steps that, over a period of more than a year, took more than 2,000 CPU hours on a Cray C-90, which is why we have decided to report on our results now instead of waiting for our simulation to span a much longer period of time. With only one reversal simulated we cannot yet say anything about the statistical behaviour of reversals in our model. Some minor changes in our model would also bring it closer to geophysical reality. But because our simulation is self-consistent and maintains a field that resem-

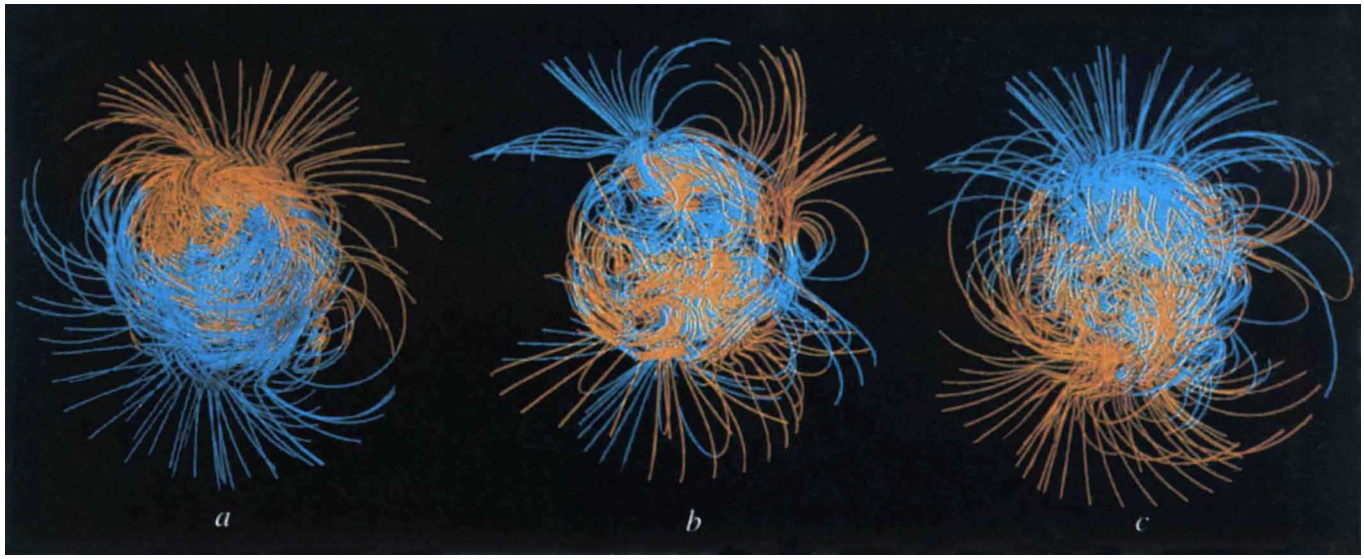

FIG. 1 The three-dimensional (3D) magnetic field structure portrayed through lines of force plotted out to the surface of our modelled Earth. Snapshots are displayed: *a*, before the reversal (9,000 years before the end of our simulation); *b*, midway through the transition as seen at the surface (that is, when the axial dipole part of the field at the surface goes through zero, about 4,000 years before the end); *c*, after the reversal (at the end of our simulation). Lines are yellow (blue) where the radial component of the field is directed outward (inward). The rotation axis is vertical. One hundred lines of force are plotted in each snapshot, so the relative field intensity is not represented in this figure.

bles the Earth's in many respects, we believe that it provides a plausible description of the geomagnetic field and the way it reverses.

Model description

The numerical model (G.A.G., manuscript in preparation) solves the nonlinear MHD equations that govern the three-dimensional structure and evolution of an electrically conducting fluid undergoing thermal convection in a rapidly rotating spherical shell, our model of the Earth's outer fluid core. A specified heat flux at the inner core boundary (ICB) drives thermal convection in the fluid core. This convection, influenced by the rotation of the core, twists and shears magnetic field, generating new magnetic field to replace that which diffuses away. The field diffuses into a solid, electrically conducting, inner core providing magnetic torque between the inner and outer cores. Magnetic torque also exists between the outer fluid core and a solid mantle above through a thin conducting layer at the core–mantle boundary (CMB). The rest of the mantle is assumed to be an insulator, so the field above this layer is a source-free potential field. Time-dependent rotation rates of the solid inner core and solid mantle are determined by the net torques at the ICB and CMB, respectively.

The model prescriptions[30] (mass, dimensions, rotation rate and material properties) are Earth-like, except the applied heat flux at the ICB, which is somewhat higher to compensate for the lack of compositional buoyancy sources in this version of our model, and the viscosity of the fluid core, which owing to computational limitations was chosen to be larger than the Earth's. But because the viscous forces in our model (outside the thin viscous boundary layers) are already about six orders of magnitude smaller than the Coriolis and Lorentz forces, our solution is probably in the correct asymptotic regime for the Earth. In comparison with two other strong-field dynamos, Kageyama *et al.*[29] assume that the convecting fluid is a compressible gas with a viscosity more than two orders of magnitude greater than our viscosity (when scaled appropriately, using the Earth's rotation rate and core radius), and St Pierre[23] uses a viscosity slightly larger than in our model.

The electrical conductivity of the solid inner core is probably much the same as that of the fluid outer core but, in our initial test calculations (those done before the simulation we are reporting on here), we assumed for simplicity an insulating inner core. The result was a chaotic magnetic field that, unlike the Earth's, reversed its dipole polarity roughly every thousand years. Hollerbach and Jones[9] then demonstrated, in their two-dimensional mean-field dynamo model, that a finitely conducting solid inner core provides a degree of stability to the magnetic field. Their alpha–omega dynamo generates a field that never reverses, although the magnetic energy undergoes periodic changes. The lack of field reversals in their solution is probably because of the particular prescription of their alpha and omega driving terms that are held constant in time. But the reversal inhibition they demonstrated and the reversal mechanism they suggested motivated us to include a finitely conducting inner core in our three-dimensional convective model. Again, in comparison, Kageyama *et al.*[29] do not have a finitely conducting inner core and therefore have no magnetic coupling between their outer and inner cores, and the model by St Pierre[23] is planar.

Our present solution, with a finitely conducting inner core, spans >40,000 years, more than three magnetic diffusion times, with no indication that it will decay away, which is suggestive evidence that our solution is a self-sustaining convective dynamo. The solution begins with random small-scale temperature perturbations and a seed magnetic field. After an initial period of adjustment (~10,000 years) during which the dipole part of the field gradually becomes dominant, our time-dependent solution maintains its dipole polarity until near the end of the simulation, when it reverses in little more than 1,000 years and then maintains the new dipole polarity for roughly the remaining 4,000 years of the simulation.

Field structure during the reversal

To illustrate the magnetic field reversal mechanism, we display the change in the structure of the field during the last 9,000 years of our simulation with three snapshots in each of Figs 1–4. The three-dimensional field structure is portrayed in Fig. 1 via lines of force at 9,000 years before the end of our simulation (Fig.

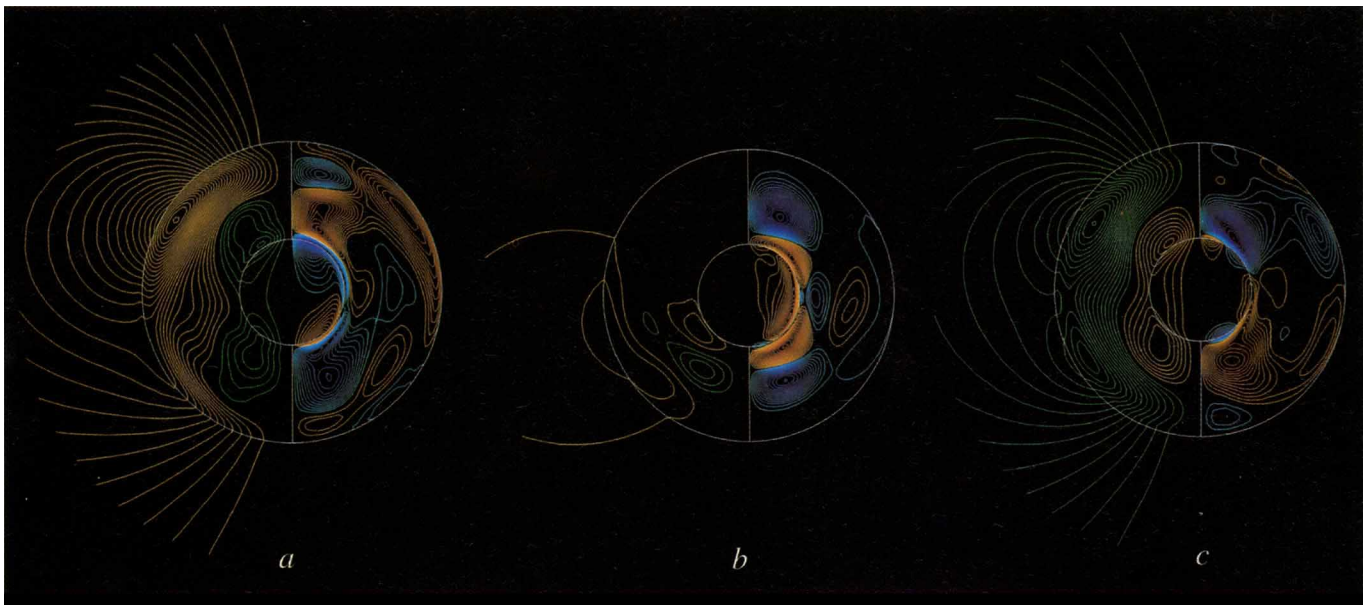

FIG. 2 The longitudinal average of the 3D magnetic field displayed with contours of the toroidal (east–west) part of the field plotted in the right hemispheres and lines of force of the meridional (poloidal) part of the field plotted in the left hemispheres. Snapshots are displayed: *a*, before the reversal (9,000 years before the end of our simulation); *b*, midway through the transition as seen at the ICB (that is, when the axial dipole part of the field at the ICB goes through zero, about 5,000 years before the end); *c*, after the reversal (at the end of our simulation). The north (south) geographic pole is at the top (bottom) of each plot. The outer circular boundary is the core–mantle boundary and the inner circular boundary is the inner core boundary. Red (blue) contours are eastward (westward)-directed toroidal field. Green (yellow) lines of force are clockwise (anticlockwise)-directed poloidal field that are plotted out to the surface. Note that for the series of plots in this figure the relative field intensity is represented in terms of the number of toroidal field contours and the density of poloidal field lines.

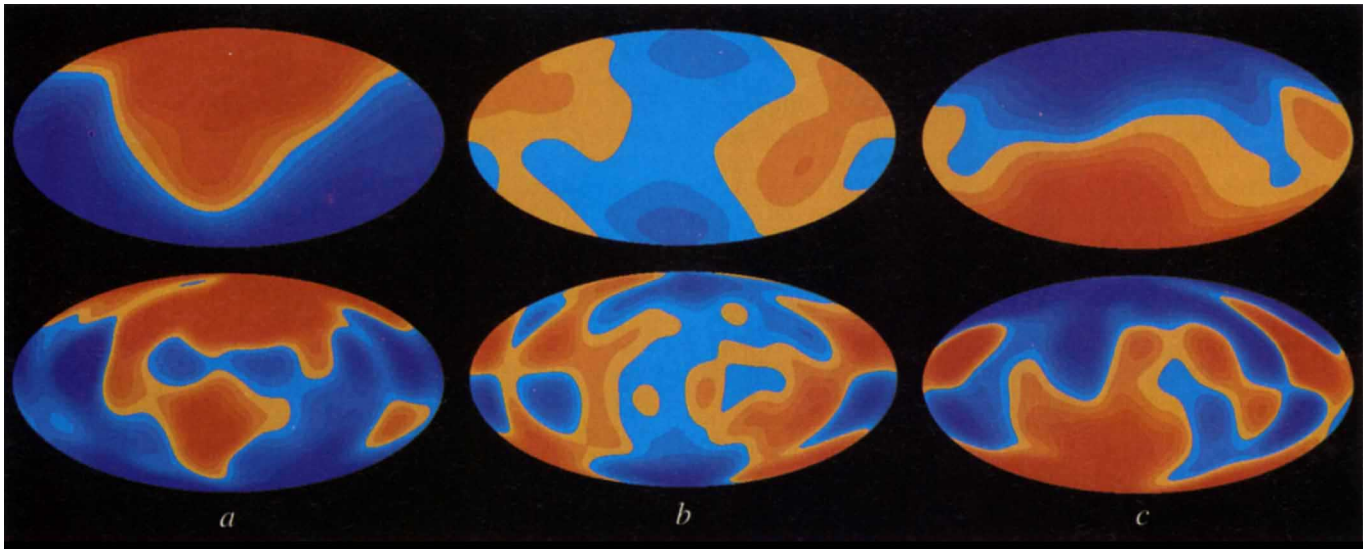

FIG. 3 The radial component of the magnetic field plotted in a Hammer projection of the core–mantle boundary (lower plots) and of the surface (upper plots). Snapshots *a*, *b* and *c* are displayed at the same times as those in Fig. 1. Red (blue) contours represent outward (inward)-directed field. The relative intensities at the different times are also reflected in the colour contours. But the field intensity at the surface has been multiplied by a factor of ten to obtain colours in the surface plots that are comparable to those in the CMB plots.

1*a*), at roughly the middle of the polarity transition as seen at the surface (~4,000 years before the end; Fig. 1*b*), and at the end of our simulation (Fig. 1*c*). We begin plotting the lines of force at the surface of our modelled Earth. They penetrate inward through the insulating mantle and then into the outer fluid core where the field is generated. The transition from the relatively smooth structure of the potential field outside the core to the much more complicated and intense field structure inside the core is quite striking. The maximum field intensity usually occurs near the ICB and is typically between 30 and 50 mT. The field at the surface has a dominantly dipolar structure before (Fig. 1*a*) and after (Fig. 1*c*) the reversal, with the dipole axis nearly aligned with the rotation axis, which is vertical in Fig. 1. During the polarity transition (Fig. 1*b*) the field structure at the

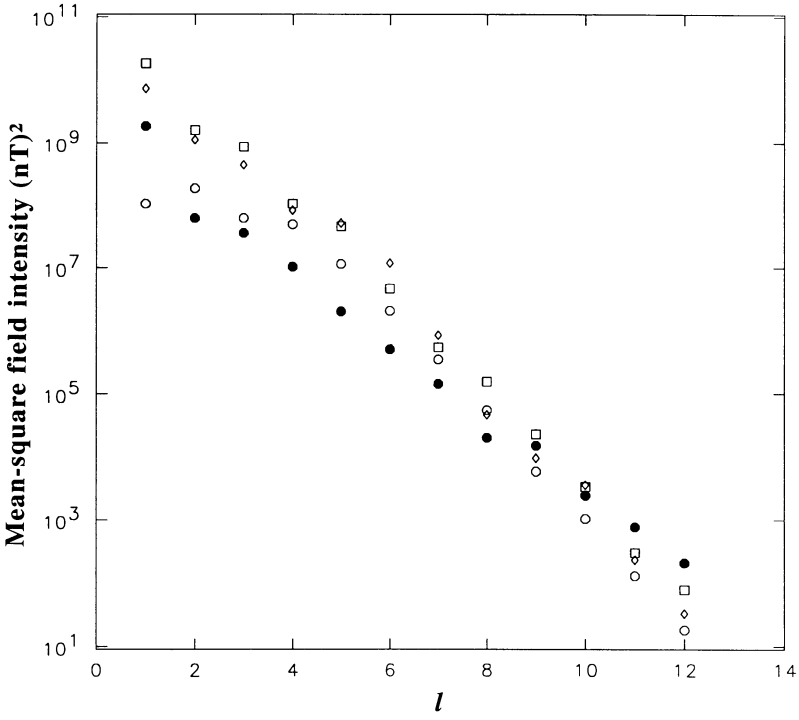

FIG. 4 The mean-square field intensity over the surface plotted as $(l+1)\Sigma_m[(g_l^m)^2+(h_l^m)^2]$, where g_l^m and h_l^m are the traditional Gauss coefficients for the potential field outside the core, and l and m are the degree and order, respectively, in the spherical harmonic expansion. Spectra are displayed at the same three times as those in Figs 1 and 3: squares before, open circles during, and diamonds after the reversal. The spectrum for the present-day Earth, based on MAGSAT data[34], is plotted as filled circles.

surface is much more complicated and the dipole axis passes through the equatorial plane.

To illustrate the field structure within the inner and outer cores more easily, we plot in Fig. 2 the longitudinal average of the three-dimensional field at 9,000 years before the end (Fig. 2*a*), at roughly the middle of the polarity transition as seen at the ICB (~5,000 years before the end; Fig. 2*b*), and at the end of our simulation (Fig. 2*c*). The right side of each plot shows contours of the east–west (toroidal) part of the field; the left side shows lines of force of the meridional (poloidal) part of the field. There are typically two main toroidal field concentrations, one in each hemisphere, in opposite directions and usually inside the imaginary cylinder tangent to the inner core where large zonal flows shear poloidal field, so generating toroidal field. Toroidal field also diffuses into the inner core from the ICB, where it is generated when poloidal field is sheared by the inner core as it moves differentially with respect to the fluid just outside the ICB.

The longitudinally averaged poloidal field (left sides of Fig. 2) typically has two dipolar polarities: one in the outer part of the fluid core, which is also the dipole polarity observed at the surface, and the opposite polarity in the inner part of the fluid core and the inner solid core. Poloidal field is generated by helical flow that twists toroidal field; in the Northern Hemisphere, for example, the time-dependent helicity of the flow (that is, the correlation between velocity and vorticity) is usually right-handed and much larger inside the 'tangent cylinder' and left-handed outside[30]. This illustrates one of the limitations of models that require, unlike ours, a prescription of the fluid flow instead of solving for it self-consistently. For example, the helical flow structure prescribed by Hollerbach and Jones[9] has no radial or time dependence and the field has only a single dipole polarity that never reverses. By contrast, it is the interaction of the two dipolar polarities present in our solution that plays an essential role in our reversal mechanism in a way that brings to mind the simple interaction between the two disks of the Rikitake dynamo model[31].

A movie of our simulation shows how the field in the fluid outer core is continually attempting to reverse its axial dipole polarity on a short timescale (~100 years) corresponding to convective overturning but usually fails because the field in the solid inner core, which can only change on a longer diffusive timescale (~1,600 years), usually does not have enough time to diffuse away before it is regenerated at the ICB. It also shows how the axial quadrupole part of the outer field tends to reverse its polarity on a roughly thousand-year timescale, causing a hemispheric (non-reversing dipole) oscillation in the structure and intensity of the outer poloidal field[10] because the sum of an axial dipole and an axial quadrupole results in an enhanced axial poloidal field in one hemisphere and a diminished poloidal field in the other. Once in many attempts the three-dimensional configurations of the buoyancy, flow and magnetic fields in the outer core are right for a long enough period of time for the inner core axial dipole field to diffuse away (Fig. 2*b*), thus allowing the reversed axial dipole polarity in the outer core to diffuse into the inner core. If this one model is representative of the Earth, it suggests that the strong nonlinear feedbacks in three dimensions and the different timescales of the fluid and solid cores are responsible for the Earth's stochastic reversal record.

When the reversal occurs in our simulation, the energy of the total field in the core is about one-quarter of its typical value. Once the new field polarity has become established, the magnetic energy in the fluid core quickly recovers. During the transition, eastward and westward toroidal field are alternately generated several times in both hemispheres at the ICB before the reversed polarity finally becomes established. Notice how the toroidal field is asymmetric with respect to the Equator before (Fig. 2*a*) and after (Fig. 2*c*) the transition but is symmetric midway through the transition (Fig. 2*b*). In our simulation, the toroidal field reverses first, then the inner poloidal field that penetrates the solid core, and finally, somewhat later, the outer poloidal field that appears at the Earth's surface reverses. This entire process takes (depending on how one defines the beginning and end of the reversal) a little more than 1,000 years, roughly the characteristic magnetic diffusion timescale for the inner core.

Figure 3 shows snapshots of just the radial component of the field plotted at the CMB (lower plots) and at the surface (upper plots) at the same three times as those depicted in Fig. 1. Because the dipolar part of the pattern decays the most slowly with radius, its contribution is greater at the surface than at the CMB. The dipole parts of these fields are nearly axial before (Fig. 3*a*) and after (Fig. 3*c*) the transition and equatorial midway through

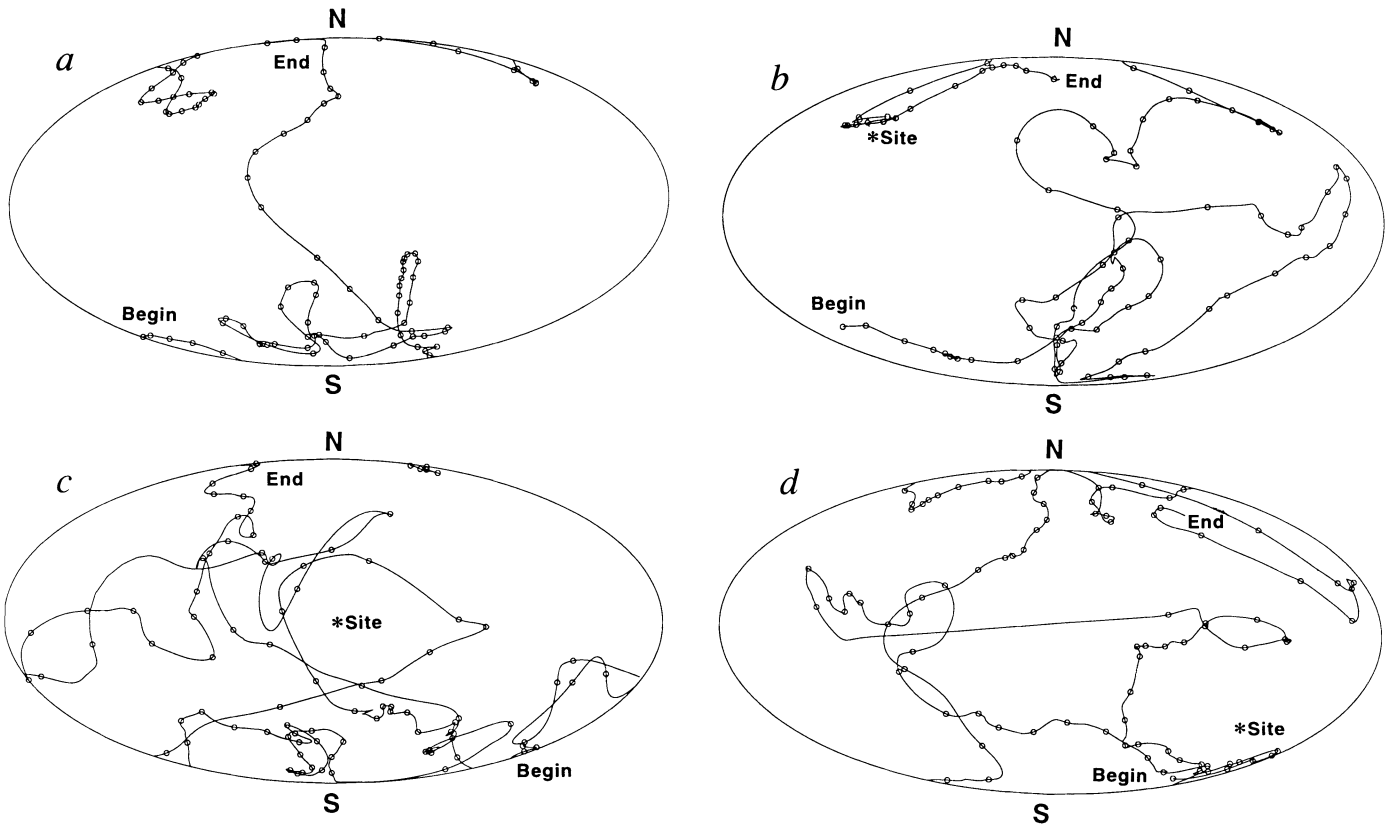

FIG. 5 The true geomagnetic pole (*a*) and the virtual geomagnetic poles (*b–d*) computed using the field directions at three surface sites: *a*, +40° latitude and 60° longitude, *b*, 0° latitude and 180° longitude, and *c*, −40° latitude and 300° longitude. The pole, with the inward-directed field, is plotted in a Hammer projection of the surface with markers at 100-year intervals during the last 9,000 years of our simulation.

the transition (Fig. 3*b*). But the dipole part of the field decreases more during the transition than the other modes do; therefore the equatorial dipole part of our transitional field is less dominant than the axial dipole part typically is before and after the transition. For example, the large radial fields at the poles in Fig. 3*b* are the result of a relatively strong quadrupole mode.

The CMB plots of Fig. 3*a*, *c* are qualitatively similar to the Earth's present field projected onto the CMB[32] with multimode contributions and several flux concentrations. The maximum intensity of the radial component of the field at the CMB in Fig. 3*a*, *c* is ~3.0 mT; the maximum intensity in Fig. 3*b* is 0.8 mT. These values can be compared with the maximum intensity of the Earth's present radial field at the CMB (ref. 32), which is ~1.0 mT.

Our simulated field structure at the surface can be compared with the Earth's present surface field stucture by plotting the mean-square field intensity over the surface as a function of the spherical harmonic degree, with the traditional Gauss coefficients[33,34]. The spectra (displayed only out to spherical harmonic degree 12) at the same three times as those used in Figs. 1 and 3 are plotted in Fig. 4. The spectra corresponding to the snapshots long before (squares) and long after (diamonds) the transition show the dipolar ($l=1$) contribution dominant over the quadrupolar ($l=2$) and octupolar ($l=3$) contributions. These two spectra indicate that we could be driving the convection a little too hard because our magnetic energies for the low degrees are higher than those of the present-day Earth[33,34], which are plotted as filled circles in Fig. 4. Also, because we have no

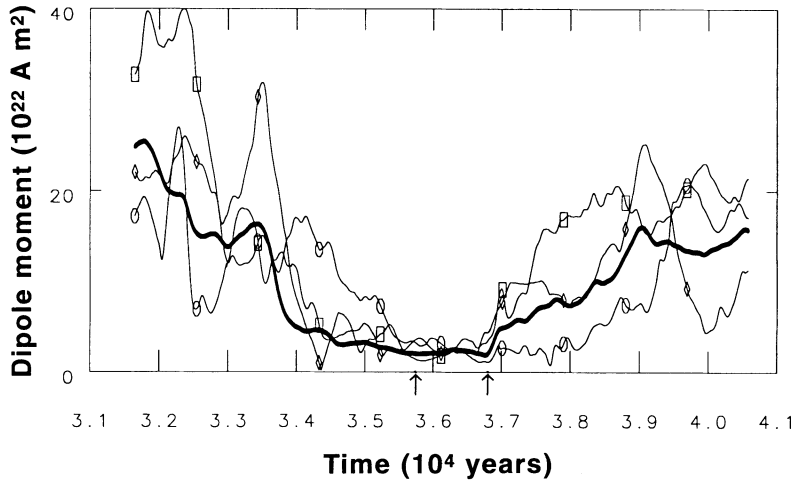

FIG. 6 The true dipole moment (heavy curve) and virtual dipole moments (marked by squares, circles and diamonds) computed using the field at the three sampling sites used in Fig. 5 during the last 9,000 years of our simulation. The times indicated are from the beginning of our simulation. The left arrow marks the mid-point in the transition as seen at the ICB, and the right arrow marks the mid-point as seen at the surface.

crustal magnetic fields in our model, the slopes of our spectra do not become shallower with increasing degree above $l=12$ (not shown), in contrast with the Earth's[33,34]. Our spectrum taken midway through the transition (open circles) shows that the dipole contribution has decreased more than the other modes during the reversal, as is also apparent in Fig. 1. During our entire simulation, magnetic energy is continually being exchanged in a chaotic manner between the modes, especially back and forth between the dipole ($l=1$) and quadrupole ($l=2$) modes on a few-thousand-year timescale. Could the decrease in the Earth's dipole moment over the past 150 years[34] be a similar adjustment?

The reversal sampled at different sites

To compare our simulated reversal with the palaeomagnetic reversal record we now describe how our reversal appears as observed locally at different sampling sites at the surface. We have analysed directional plots (declination and inclination) of our surface field at 50 sites distributed over the surface spanning the last 9,000 years of the simulation. These plots (not shown) indicate that the evolution of the local field direction depends greatly on the sampling location; but they all show that a reversal has occurred. By monitoring the rate of change of our surface field direction at these 50 sites we find the largest rate (at one site, at one time) to be 0.1° per day. But most sites have a maximum rate of ~0.01° per day during the reversal, which is larger than the rate observed in the secular variation of the present-day geomagnetic field[34] but much less than the impulse of 6° per day inferred from the Steens Mountain record[35], the largest rate seen in the palaeomagnetic reversal record.

By knowing the local direction of the surface field at a sampling site (that is, declination and inclination) and assuming the field to be purely dipolar, one can determine the geographical location of the virtual geomagnetic pole (VGP)[3]. In our model we can isolate just the dipolar part of the field (that is, spherical harmonics of degree $l=1$) and compute the geographical location of the true geomagnetic pole (TGP), a luxury that palaeomagnetists do not enjoy owing to the relatively sparse set of sampling sites and the uncertainty in correlating the ages of samples from the different sites. The TGP path (Fig. 5*a*) during the last 9,000 years of our simulation shows several excursions (or aborted reversals)[36] occurring at different longitudes before and after the successful dipole reversal occurs. The transition itself, seen in our TGP path, takes only ~1,200 years (depending on how one defines the beginning and end of the transition) compared with estimates that range from 1,200 years to the more likely ~5,500 years, seen in the palaeomagnetic reversal record[35,37,38].

We have plotted in Fig. 5*b–d* the VGP paths over the surface during the last 9,000 years of our simulation at three arbitrary sampling sites. Although these VGP paths show that a reversal has occurred, the details are strongly dependent on the sampling site (marked by an asterisk) and do not resemble the TGP path. For example, the long, nearly horizontal, 100-year segment of the VGP path in Fig. 5*d* corresponds to an 'impulse' that is also seen in the directional plot at the same site but is not seen in the other VGP paths or in the TGP path. In addition, our estimate of the transition time would be significantly longer than 1,200 years if we based it only on these VGP paths.

These plots can be compared with VGP transition paths or patches from the palaeomagnetic record, which some argue occur at preferred longitudes[36,39,42] and others interpret in other ways[43–47]. But because the boundary conditions at the ICB and CMB in our present simulation are spherically symmetric, we do not and would not expect to see our excursions and transition occur along preferred longitudes[41,48,49], although we do intend to investigate this intriguing issue with modified versions of our model.

If, in addition to measuring the inclination and declination, one measures the field intensity at a given sampling site, the virtual dipole moment (VDM) of the assumed dipolar field can be computed[3]. In Fig. 6 we plot the VDM computed with the field at our same three sampling sites during the last 9,000 years of our simulation. Also plotted in Fig. 6 is our true dipole moment (TDM). The VDMs provide crude approximations to the TDMs; they correctly reflect the general decrease of the TDM before and during the transition and the recovery after the transition, which is similar to what is seen in palaeointensity records[3]. An asymmetric 'saw-tooth' pattern is also seen in filtered palaeointensity records[50] but the typical time constant of the cycles is ~500,000 years, much longer than the time of our simulation spans. It is interesting that our TDM decreases to nearly its minimum value almost 2,000 years before the mid-point in the transition as seen at the ICB (the left arrow in Fig. 6). It remains low until the mid-point in the transition as seen at the surface (the right arrow in Fig. 6), when it begins its recovery. It is typically between 10×10^{22} and 20×10^{22} A m^2 during most of the simulation, compared with the Earth's present value of $\sim8\times10^{22}$ A m^2. It reaches a minimum of 1.6×10^{22} A m^2 midway through the transition, which is ~10% of its usual value compared with the average drop to 25% seen in plots of the VDM for the Earth[3].

The relatively poor correlations in Figs 5 and 6 between the three sampling sites are due to the fact that the dipole contribution in our simulated magnetic field is not always strongly dominant (Fig. 4). This illustrates how uncertain the details of the VGPs and VDMs could be if the Earth's field were not strongly dipolar during its reversals as some palaeomagnetic reversal records suggest[44,51].

Model limitations and needed improvements

With these initial results from our self-consistent global three-dimensional simulation of the geodynamo we have attempted to bridge the palaeomagnetic and dynamo modelling communities. But with so far only one reversal simulated, our explanations and conclusions about geomagnetic reversals are speculative. Certainly, more analysis is required to improve our understanding of the geodynamo and its reversal mechanism. In addition, several model improvements, which could alter our results and conclusions, will be required for more realistic simulations in the future. For example, more detailed thermodynamics, including compositional convection, is needed. The viscous, thermal and compositional eddy diffusivities should be variable and anisotropic. The effects of topography at the CMB, heterogeneous heat flux and electrical conductivity at the CMB, and luni-solar precession of the mantle could also provide interesting new insights. □

Received 16 June; accepted 23 August 1995.

1. Elsasser, W. M. *Phys. Rev.* **72,** 821–833 (1947).
2. Parker, E. N. *Astrophys. J.* **122,** 293–314 (1955).
3. Merrill, R. T. & McElhinny, M. W. *The Earth's Magnetic Field* (Academic, London, 1983).
4. Cowling, T. G. *Mon. Not. R. astr. Soc.* **94,** 34–48 (1934).
5. Roberts, P. H. & Soward, A. M. *A. Rev. Fluid Mech.* **24,** 459–512 (1992).
6. Braginsky, S. I. & Roberts, P. H. *Geophys. astrophys. Fluid Dyn.* **38,** 327–349 (1987).
7. Olson, P. *Geophys. Res. Lett.* **16,** 613–616 (1989).
8. Barenghi, C. F. & Jones, C. A. *Geophys. astrophys. Fluid Dyn.* **60,** 211–243 (1991).
9. Hollerbach, R. & Jones, C. A. *Nature* **365,** 541–543 (1993).
10. Glatzmaier, G. A. & Roberts, P. H. *J. Geomag. Geoelectr.* **45,** 1605–1616 (1993).
11. Nakajima, T. & Roberts, P. H. *Proc. R. Soc. Lond.* A **448,** 1–28 (1995).
12. Pekeris, C. L., Accad., Y. & Shkoller, B. *Phil. Trans. R. Soc. Lond.* A **275,** 425–461 (1973).
13. Kumar, S. & Roberts, P. H. *Proc. R. Soc. Lond.* A **314,** 235–258 (1975).
14. Gubbins, D. & Sarson, G. *Nature* **368,** 51–55 (1994).
15. Zhang, K. K. & Busse, F. H. *Phys. Earth planet. Inter.* **59,** 208–222 (1990).
16. Arter, W. *Geophys. astrophys. Fluid Dyn.* **31,** 311–344 (1985).
17. Matthews, P. C. in *Solar and Planetary Dynamos* (eds Proctor, M. R. E., Matthews, P. C. & Rucklidge, A. M.) 211–218 (Cambridge Univ. Press, 1993).
18. Fearn, D. R., Proctor, M. R. E. & Sellar, C. C. *Geophys. astrophys. Fluid Dyn.* **77,** 111–132 (1994).
19. Olson, P. & Glatzmaier, G. A. *Phys. Earth planet. Inter.* (in the press).
20. Meneguzzi, M. & Pouquet, A. *J. Fluid Mech.* **205,** 297–318 (1989).
21. Brandenburg, A., Nordlund, A., Pulkkinen, P., Stein, R. F. & Tuominen, I. *Astr. Astrophys.* **232,** 277–291 (1990).
22. Nordlund, A. *et al. Astrophys. J.* **392,** 647–652 (1992).
23. St Pierre, M. G. in *Solar and Planetary Dynamos* (eds Proctor, M. R. E., Matthews, P. C. & Rucklidge, A. M.) 295–302 (Cambridge Univ. Press, 1993).
24. Gilman, P. A. & Miller, J. *Astrophys. J. Suppl.* **46,** 211–238 (1981).
25. Gilman, P. A. *Astrophys. J. Suppl.* **53,** 243–268 (1983).

26. Glatzmaier, G. A. *J. comput. Phys.* **55,** 461–484 (1984).
27. Glatzmaier, G. A. *Astrophys. J.* **291,** 300–307 (1985).
28. Glatzmaier, G. A. *Geophys. astrophys. Fluid Dyn.* **31,** 137–150 (1985).
29. Kageyama, A. *et al. Phys. Plasmas* **2,** 1421–1431 (1995).
30. Glatzmaier, G. A. & Roberts, P. H. *Phys. Earth planet. Inter.* **91,** 63–76 (1995).
31. Rikitake, T. *Proc. Camb. phil. Soc.* **54,** 89–105 (1966).
32. Bloxham, J. & Gubbins, D. *Nature* **317,** 777–781 (1985).
33. Cain, J. C., Wang, Z., Schmitz, D. R. & Meyer, J. *Geophys. J.* **97,** 443–447 (1989).
34. Langel, R. in *Geomagnetism* (ed. Jacobs, J. A.) Vol. 1, 249–512 (Academic, San Diego, 1987).
35. Coe, R. S., Prevot, M. & Camps, P. *Nature* **374,** 687–692 (1995).
36. Hoffman, K. A. *Nature* **359,** 789–794 (1992).
37. Opdyke, N. D., Kent, D. V. & Lowrie, W. *Earth planet. Sci. Lett.* **20,** 315–324 (1973).
38. Kristjansson, L. *Geophys. J. R. astr. Soc.* **80,** 57–71 (1985).
39. Tric, E. *et al. Phys. Earth planet. Inter.* **65,** 319–336 (1991).
40. Clement, B. M. *Earth planet. Sci. Lett.* **104,** 48–58 (1991).
41. Laj, C., Mazaud, A., Weeks, R., Fuller, M. & Herrero-Bervera, E. *Nature* **351,** 447 (1991).
42. Ratcliff, C. D., Geissman, J. W., Perry, F. V., Crowe, B. M. & Zeitler, P. K. *Science* **266,** 412–416 (1994).
43. Langeres, C. G., van Hoof, A. A. M. & Rochette, P. *Nature* **358,** 226–230 (1992).
44. Valet, J.-P., Tuchloka, P., Courtillot, V. & Meynadier, L. *Nature* **356,** 400–407 (1992).
45. McFadden, P. L., Barton, C. E. & Merrill, R. T. *Nature* **361,** 342–344 (1993).
46. Prevot, M. & Camps, P. *Nature* **366,** 53–57 (1993).
47. McFadden, P. L. & Merrill, R. T. *J. geophys. Res.* **100,** 307–316 (1995).
48. Runcorn, S. K. *Nature* **356,** 654–656 (1992).
49. Clement, B. M. & Stixrude, L. *Earth planet. Sci. Lett.* **130,** 75–85 (1995).
50. Valet, J.-P. & Meynadier, L. *Nature* **366,** 234–238 (1993).
51. Clement, B. M. & Kent, D. V. *Geophys. Res. Lett.* **18,** 81–84 (1991).

ACKNOWLEDGEMENTS. The computing resources for this simulation were provided by the NSF Pittsburgh Supercomputing Center. Support for this research was provided by the Institute of Geophysics and Planetary Physics and the LDRD program at Los Alamos.

Transcription complex stability and chromatin dynamics *in vivo*

Mark Wijgerde*, Frank Grosveld*† & Peter Fraser*

* MGC Department of Cell Biology and Genetics, Erasmus University, 3015 GE Rotterdam, The Netherlands
† Laboratory of Gene Structure and Expression, National Institute for Medical Research, The Ridgeway, Mill Hill, London NW7 1AA, UK

Distant regulatory sequences affect transcription through long-range chromatin interactions. Visualization of transcriptional activity of genes that compete for distant elements, using the globin locus as a model, has revealed the dynamics of chromatin interactions *in vivo*. Multiple genes appear to be transcribed alternately rather than at the same time to generate several messenger RNAs in one cell. The regulator may stably complex with one gene at a time and switch back and forth between genes in a flip-flop mechanism.

MANY genes are dependent for expression on the presence of distant regulatory elements which may be tens of thousands of base pairs away. The five human β-globin genes are arranged in the order of their developmental expression (ε-Gγ-Aγ-δ-β)[1] and all are dependent on the locus control region (LCR) for high-level, position-independent expression[2–4]. The LCR is located over 50 kilobases (kb) upstream of the β-globin gene and consists of five DNaseI-hypersensitive sites (HS)[3,5–7]. The most important sites in terms of transcriptional activation are HS 2–4 (refs 8, 9 and J. Ellis *et al.*, manuscript submitted), each having a core region of 200–300 base pairs (bp)[10–14].

Transcriptional competition between genes[15,16] is important *in vivo* in determining the pattern of globin gene expression during development[17–20] (N. Dillon *et al.*, manuscript submitted). All of the genes are in polar competition for the activating function of the LCR at all stages of development, with proximal genes having an advantage over distal genes, suggesting that the LCR interacts directly with the gene(s) by a looping mechanism.

The distal β-globin gene is transcriptionally competent at all stages of development, but its expression is suppressed in embryonic erythroid cells by the LCR proximal ε- and γ-globin genes. Expression of the β-gene occurs only after silencing of the ε- and γ-genes, presumably by multiple silencing elements in the sequences immediately flanking the genes[21–23]. In contrast to models proposing that different HS regions of the LCR interact with different genes at the same time[24], we have proposed that the LCR HS elements interact to act together or form a holocomplex which then interacts with proximal transcriptionally competent genes via looping (ref. 9 and J. Ellis *et al.*, submitted). The LCR holocomplex model would explain why the activity of the HS is additive and why each of the genes requires all of the HS for full expression. Most important, it would explain the fact that there is balanced competition between the genes for LCR function. A key question in validating this model is whether the LCR is limited to activating only a single gene at a time or, as others suggest, the LCR splits its function[24] and activates several genes simultaneously[25,26]. We have addressed this question by *in situ* hybridization analysis of the erythroid tissues derived from a transgenic mouse line carrying a single copy of the complete human β-globin locus. The results show that the LCR activates only one gene at a time, indicating that the LCR–globin-gene interaction is monogenic. Furthermore, these interactions are not static, but dynamic, with transcription interactions forming, breaking and reforming in a type of flip-flop mechanism. Finally, the average stability of the LCR–gene interactions was estimated to be of the order of 15–80 min.

Globin primary transcripts

Analysis of γ- and β-globin steady-state messenger RNA levels during switching in the early stages of transgenic fetal liver erythropoiesis (11.5–13.5 d) show that both are detectable in total fetal liver RNA[27], with γ-gene expression decreasing and β-globin gene expression increasing. Both γ- and β-globin polypeptides occur in most cells of the transgenic fetal liver[9,28], indicating that commitment to γ- or β-gene expression does not occur before the onset of globin transcription. The detection of globin mRNA or polypeptides are not reliable indicators of concurrent transcriptional activity in developing cells owing to the long half-lives of such molecules. Alternatively, primary transcripts are both temporally and spatially associated with the transcriptional event and have short half-lives due to rapid splicing into mature mRNA. The half-life of the mouse β-major globin primary transcript has been calculated to be <5 min in mouse erythroleukaemia cells[29]. Detection of primary transcripts *in situ* is therefore an accurate indicator of ongoing or very recent transcription. If transcription complexes last longer than the half-life of the primary transcript, two types of signals may occur: single-gene transcription signals or multigene signals. Whereas the explanation for the single-gene signal is obvious, the multigene signal could result from either of two events, namely concurrent transcription from two genes or a recent switch causing a signal overlap between transcription from one